SAXS Study Applied to Reversibly Crosslinked Isotactic Polypropylene/Clay Nanocomposites

S. Bouhelal,[1] M. E. Cagiao,[2] D. Benachour,[1] B. Djellouli,[3] L. Rong,[4] B. S. Hsiao,[4] F. J. Baltá-Calleja[2]

[1]*LMPMP, Faculty of Engineering, Ferhat Abbas University, Sétif, Algeria*
[2]*Department of Macromolecular Physics, Instituto de Estructura de la Materia, CSIC, Madrid 28006, Spain*
[3]*LGPC, Faculty of Engineering, Ferhat Abbas University, Sétif, Algeria*
[4]*Department of Chemistry, State University of New York, Stony Brook, New York 11794-3400*

Received 8 September 2009; accepted 5 February 2010
DOI 10.1002/app.32241
Published online 3 May 2010 in Wiley InterScience (www.interscience.wiley.com).

ABSTRACT: A new route based on reversibly crosslinking reactive extrusion is applied for the development of iPP/clay nanocomposites. Analysis of small-angle X-ray scattering (SAXS) reflections of isotactic polypropylene (iPP)/clay nanocomposites, prepared by two different mixing and chemical crosslinking methods (i.e., conventional and *in situ*), is presented and results are compared with preceding wide-angle X-ray diffraction (WAXD) results. It is shown that the presence of clay significantly affects the value of long spacing in iPP, as well as the coherence length of lamellar stacks. Results show that the size of the coherently diffracting nanodomains decreases in two stages, first rapidly and then slowly as a function of increasing clay content. This can be attributed to the influence of confined iPP lamellae under the effect of rising number of clay particles. The appearance of the γ-crystalline form in the crosslinked iPP/clay nanocomposites is related with the difficulty in chain folding of iPP chains introduced by the chemical crosslinking process, as well as by the presence of clay particles. © 2010 Wiley Periodicals, Inc. J Appl Polym Sci 117: 3262–3270, 2010

Key words: isotactic polypropylene; clay nanocomposites; reversible crosslinking; polymorphism; X-ray scattering

INTRODUCTION

Nanocomposite technologies, which have been quickly developed in the last years, are among one of the most promising areas of plastics industry today.[1] One of the main advantages of these technologies is their applicability to almost every kind of polymers. Polymer/clay nanocomposites are one of the more widely studied systems,[2–4] especially when they present intercalated or exfoliated phases, which give rise to enhanced properties, such as conductivity,[5] low gas-barrier properties,[6,7] etc. These properties, obtained with clay concentrations of 5% or even less, are related to enormous interfacial adhesion regions that characterize the nanocomposites. Several reviews[8–10] have appeared in recent years describing the different methods developed for the preparation and processing of polymer–clay nanocomposites. The contribution of Sinha Ray and Okamoto[10] covers different kinds of polymers used to prepare polymer/clay nanocomposites, the main methods developed for their preparation, characterization techniques used, and most relevant properties of such materials. One of the clay types most widely studied is the montmorillonite. It belongs to the kind of the so-called 2 : 1 layered- or phyllo-silicates. Its crystal structure is formed by two tetrahedral layers of silica fused to an edge-shared octahedral sheet of either aluminium or magnesium hydroxide.[8,11] The stacked layers leave a regular Van der Waals gap between them, called interlayer space or gallery. This gap is usually occupied by hydrated Na^+, K^+, or Ca^{2+} cations.[11]

We are particularly interested in the preparation of isotactic polypropylene iPP/clay nanocomposites in our group. A frequently used method for the preparation of these nanocomposites is by melt mixing of iPP with clay.[4,11–16] However, clay, owing to its strong hydrophilic character, is incompatible with most polymers. Thus, a direct melt mixing of both components is not feasible. To overcome this difficulty, as a first step, the surface of the clay has to be modified by using an organophilic agent, thus giving rise to the so-called organophilic clay or organoclay.[11,17] After that, the melt compounding is performed either with iPP alone,[13,15] or with iPP plus some additives, i.e., functionalized monomers,[9] coupling agents, as iPP-*g*-MAH (iPP grafted with maleic

Correspondence to: F. J. Baltá-Calleja (embalta@iem.cfmac.csic.es).

Contract grant sponsor: Grant Ministry of Science and Innovation, Spain; contract grant number: FIS2007-60534.
Contract grant sponsor: National Science Foundation, USA; contract grant number: DMR-0906512.

anhydride)[4,12,14–16] etc. The compounding is made by using a polymer mixer or extruder under shear conditions. Another way to prepare polymer/clay nanocomposites is by reactive melt mixing, which generally uses a peroxide as source of oxy-radicals.[18] The peroxide decomposes under the appropriate processing conditions. However, this method still needs the use of clay that has been previously organophilized. Nevertheless, in the newest recently reported approach,[18] it is possible to prepare iPP/clay composites using untreated clay. Only a previous purification step is necessary.[19,20]

The aim of this article is to characterize a series of iPP/clay nanocomposites by means of SAXS and WAXD techniques attempting to describe the evolution of the nanostructure as a function of clay content for nanocomposites prepared by both conventional and *in situ* methods.

EXPERIMENTAL

Materials

The materials used in this investigation were the following:

- Isotactic polypropylene, iPP 05-RF03-0577 C-2807; supplied by Oriental Petrochemicals, Saudi Arabia.
- Dicumyl peroxide (DCP), 96 wt % activity; supplied by NORAX (Germany). Sulfur (S) (vulcanizing agent for rubber); supplied by Wuxi Huasbeng Chemical Additives Factory (China). Potassium persulfate; supplied by Innochem, Belgium. Potassium persulfate has already been used in some grafting polymerization methods,[21] and his role is to assist and promote the life time of the macro radicals, particularly when the efficiency of the peroxide is not so high.
- The accelerator used was "Super accelerator 501" (tetramethyl thiuram disulfide TMTD); supplied by Rhône-Poulenc, France. The peroxide, the sulfur and the accelerator constitute the "crosslinking agent".
- Concerning the clay, we used an untreated sodium montmorillonite called Maghnite, obtained from the Algerian region of Maghnia; supplied by ENOF, Algeria. The cation exchange capacity CEC of this montmorillonite is about 1.15×10^{-3} mol g^{-1}.[22]

Nanocomposite preparation

We have studied a series of composites consisting of mixtures of reversibly crosslinked iPP[23,24] plus clay, in concentrations ranging from 2 to 50 wt %. The composite preparation has been already explained in some details before.[19]

TABLE I
iPP/Clay Composition and Preparation Method of Composites

Samples	Clay content (wt %)	Preparation method
Unmodified i-PP	0	–
Crosslinked i-PP	0	–
Crosslinked i-PP	2	Conventional
Crosslinked i-PP	4	Conventional
Crosslinked i-PP	8	Conventional
Crosslinked i-PP	12	Conventional
Crosslinked i-PP	16	Conventional
Crosslinked i-PP	20	Conventional
Crosslinked i-PP	30	Conventional
Crosslinked i-PP	40	Conventional
Crosslinked i-PP	10	*In situ*
Crosslinked i-PP	50	*In situ*

Two different preparation methods, conventional and *in situ*, have been used to prepare the samples. In both methods, the clay only has to be separated from the rest of minerals or impurities by washing the raw material with distilled water followed by centrifugation. It is not necessary to perform any other chemical treatment or purification step. The dried clay (100°C, 24 h) is then screened through sieves (granular size, 63 μm or less).

For the blends preparation, the chosen sulfur concentration (in wt %) was equal to that of peroxide, and the accelerator was 1/4 of the sulfur or peroxide concentration. The crosslinking agent was added in a concentration 1/10 of the clay. The compositions of the blends are summarized in Table I. The two preparation methods are briefly explained below.

In the so-called conventional method, iPP, crosslinking agent, potassium persulfate, and dried/sieved clay, were mixed in the solid state with appropriate weight % ratios, together with a few drops of a vegetable oil, which facilitated the dispersion of the powder additives within iPP granules. The resulting mixture was subsequently introduced into a single screw laboratory extruder (Prolabo 1989) having the following characteristics: L/D = 20; screw diameter = 25 mm; screw speed: 60 turns/min; time of residence ≈ 3 min. The selected temperatures for the three stages, i.e. feed, compression, and homogenization were 155, 180, and 200°C, respectively. The composites containing from 2 to 12 wt % of clay were prepared in a single extrusion step. For the preparation of composites with 16 wt % of clay, 4% of clay was added to the sample with 12% of clay in a second extrusion step. The same procedure was used to prepare the rest of compositions. Thus, the sample with 20 wt % of clay was prepared by adding 4% of clay to the sample

having 16% of clay in a third extrusion step, and so on. This way, samples with clay content as high 40 wt % are prepared. Eight samples were prepared by this method. Compositions are indicated in Table I.

In the *in situ* method, first acetone and then dried/sieved clay were added to the crosslinking agent. The acetone volume was, at least, equal to three times the volume of the solid (total solid = crosslinking agent + clay). After a few minutes, two separate phases appeared. The solid phase contained the functionalized clay, while the liquid one contained acetone plus some impurities. After one day of mixing, the solid phase was ready to be blended with iPP in the desired amount. This way, the penetration and diffusion of the agents between the interlayer spaces of the clay was favored. It is to be noted that the main role played by the acetone at this step of the process is to protect the clay from the water absorption before the blending process takes place. The iPP and the functionalized clay have been processed in an extruder under the same processing conditions used for the conventional method. Thereafter, the acetone is released simply by evaporation. In addition, the decomposition temperature of peroxide and the activation temperature of the accelerator verified by DSC, shift down by almost 10°C. These results suggest that the clay acts as kicker.

By this method, the clay was directly functionalized by the oxy radicals originated in the decomposition of DCP. The final result was that, as a consequence of the oxy-reduction reaction that took place, the macroradicals were grafted onto the clay nanolayers. A detailed explanation of the whole process, together with the several interesting roles played by the acetone, had been already published.[19] The most relevant point of the *in situ* method is the possibility of preparing nanocomposites with clay content as high as 50 wt % in only one step. Two samples prepared by this method, containing 10 and 50 wt % of clay, were used in this study (Table I for composition). The preparation of samples with other compositions, to cover the same range as those obtained by the conventional method, is now in progress.

Characterization techniques

The iPP/clay composites included in this study were previously characterized by several methods: wide-angle X-ray diffraction (WAXD), differential scanning calorimetry (DSC), and microindentation hardness measurements.[19] The onset of the crosslinking, as indicated in,[19] was measured by the method of Harpell and Walrod.[25] It consists of a dynamical rheological analysis, used to evaluate the crosslinking degree in the molten state by measuring the crosslinking time and torque level value. It has been applied to iPP, and it is preferable than the gel content method, which is more appropriate and normalized for PE samples (the casting temperature, 110°C, is very low in contrast to the iPP melting point). In addition, the results obtained by the Harpell-Walrod method agree very well with the ones derived by the DMA rheological study, as it will be shown in a forthcoming paper.

To complete the samples characterization, small-angle X-ray scattering (SAXS) was also used in this study. The results derived from the SAXS study are analyzed and discussed together with the results previously obtained in the WAXD study.[19] As a result, a more comprehensive picture of the effect caused by the presence of clay on the morphology and structure of iPP was obtained in these two types of nanocomposites.

For the WAXD study, a Seifert diffractometer (reflection mode) was used. The following conditions were employed: Ni-filtered Cu K_α radiation, with $\lambda = 0.15418$ nm; 40 kV; 35 mA; angular range: 2–35° (2θ); scan rate: 0.02°/s; slits: 2, 1, 0.3, 0.2.

The SAXS study was performed in the beam line X27C of the National Synchrotron Light Source at Brookhaven National Laboratory, in New York. The working conditions were the following: wavelength = 0.1371 nm; sample-detector distance = 1870.4 mm. A bidimensional detector was used. Data were analyzed by means of the Fit-2d program, after averaging them in the whole angular range, i.e., 360°. Lorentz's correction was applied to all SAXS patterns, thus obtaining the plots of $I.q^2$ as a function of the wave vector $q = 2\pi s$ (where $s = 2 \sin \theta/\lambda$).

RESULTS

Wide-angle X-ray diffraction results

As it has been reported previously,[19] the WAXD pattern of all the clay-containing nanocomposite samples (except the one with 4% of clay), exhibits the typical reflections of the α-form of iPP,[26] together with two additional peaks, at 6.9 and 26.7° (2θ) (Fig. 1); the first one is characteristic of the d_{001} spacing of clay; the second one, with much less intensity, is originated by the quartz usually accompanying the clay. In addition, in almost all crosslinked iPP samples appear two peaks at 16.2 and 20.1° (2θ), respectively (Fig. 1). The peak at 16.2° (2θ) is characteristic of the (300) planes of the iPP β-crystalline form,[26] whereas the one at 20.1° (2θ) can be related to the (130) or (117) planes of the γ-crystalline modification.[27,28] Here, it is noteworthy to indicate that two different crystal cells, named II and III, have been tentatively proposed for the iPP γ-form. Thus, whereas in crystal cell II (triclinic) the reflections appearing at 16.7 and 20.1° (2θ) are assigned to the planes (040) and (130),[27] in crystal

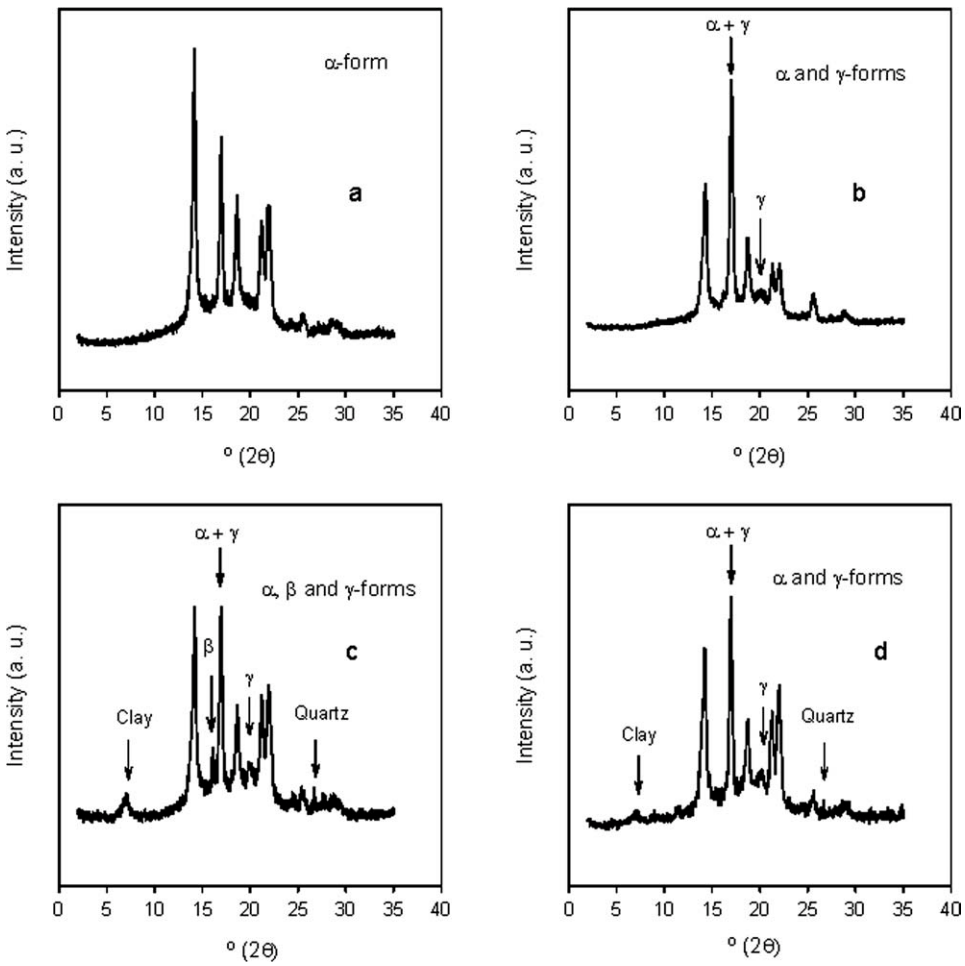

Figure 1 Diffractograms of: (a) unmodified iPP; (b) crosslinked iPP; (c) crosslinked iPP/clay nanocomposite (conventional method, 8 wt % of clay); (d) crosslinked iPP/clay nanocomposite ("*in situ*" method, 10 wt % clay).

cell III (orthorhombic) the same reflections are related to the planes (008) and (117).[28]

This γ-form is already present in the diffractogram of the crosslinked sample having no clay. In the sample with 12 wt % of clay, and in the two ones prepared by the *in situ* method, only the reflection at 20.1° (2θ) (γ-form) appears. In Figure 1 the reflections corresponding to the clay, the quartz and the β- and γ-crystalline forms of iPP are indicated by arrows.

As previously reported,[19] in all the crosslinked samples the intensity of the reflection at 16.7° (2θ) is higher than that of pristine iPP. This is also due to the appearance of the γ-crystalline form in the modified material, as both α- and γ- forms show a reflection in this position. This reflection is related to the (040) planes for iPP α-form. However, in case of γ-form, it has been tentatively assigned to the (040)[27] or (008) planes,[28] depending on the crystal cell admitted is II or III (vide supra). In what follows, we assume that the crystal cell for the iPP γ-form is Type II.[27]

Thus, we have estimated the content X_γ of the γ-form in all the studied samples according to the method of Turner-Jones et al.[29,30]:

$$X_\gamma = I^\gamma_{(130)} / \left(I^\gamma_{(130)} + I^\alpha_{(130)} \right) \quad (1)$$

where $I^i_{(130)}$ is the intensity of the (130) peak of each polymorphic form. As indicated above, the (130) peak for the γ-form appears at 20.1° (2θ), and in case of α-form, at 18.4° (2θ). The X_γ value gradually increases from 0.37 in the crosslinked sample without clay, up to 0.50 for the samples with 30–50% of clay.

Concerning the β-form, its contribution reaches the highest value in the sample with 20 wt % of clay. For this composition, the β-form represents, approximately, 8% of the total diffracted intensity, or 13% over the crystalline material.[19]

All the samples (except the one with 4 wt % of clay) show the characteristic 001 clay peak at about 6.9° (2θ) (*d*-spacing = 1.28 nm). This peak is shifted to higher diffraction angles as compared to the one appearing in the pristine, dry clay at 6.23° (2θ), (*d*-spacing = 1.42 nm).

On the other hand, if we take as a reference the main iPP peak, at 16.7° (2θ) we can see that the peak

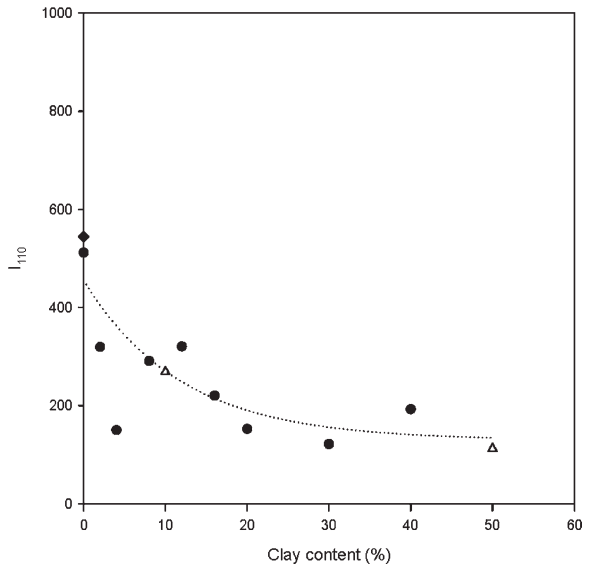

Figure 2 Intensity of the main reflection of iPP at 16.7° (2θ) as a function of clay content.

intensity gradually diminishes with increasing clay content (except for the sample with 4 wt % of clay, that shows a minimum). For the highest clay content compositions, the intensity of this peak reduces to approximately the half of the original value (Fig. 2).

Small-angle X-ray scattering results

Figure 3 shows the SAXS patterns of the unmodified iPP (named iPP0) (a), the crosslinked iPP with no clay (XiPP0) (b), and the crosslinked iPP+2 wt % of clay (XiPP2) (c). The double orientation effect is clearly visible only in the XiPP0 sample. The rest of compositions exhibit isotropic SAXS diagrams.

The original, untreated iPP and most of iPP/clay composites exhibit two SAXS maxima (Fig. 4). The values of the two long spacing obtained, L_1 and L_2, indicate that the second maximum is not related to the first one. Furthermore, after crosslinking the iPP sample develops a double orientation similar to the crossed hatched structure found in TEM studies.[31] For clay content values between 2 and 12 wt %, $L_1 \cong$ 15 nm. When the clay concentration is equal to 16 wt %, L_1 increases from 15 to 18 nm, being even higher (22.0 and 24.3 nm) for samples with of 40 and 50% of clay, respectively (Fig. 5). The intensity of the second SAXS maximum I_2 and the L_2 value are practically constant for all compositions, i.e., $L_2 \cong$ 8 nm (Fig. 5). For clay contents higher than 30 wt %, I_2 practically disappears.

To calculate the coherence length D_{SAXS} from the full width at half maximum (FWHM) of the first reflection, we have assumed the occurrence of paracrystalline distortions, originated by the three-dimensional distribution of motifs, like conformational defects, that disturb the crystalline packing.[32–35] Such distortions give rise to a decrease in the amplitude of the Bragg reflections and a nonlinear increase in the integral breadths, δβ, of successive higher order reflections (m).[32] According to the paracrystalline theory, when two or more reflections appear that correspond to different orders of the same spacing d (or L, if we are dealing with SAXS profiles), there is a linear relationship between the values of δβ derived from the FWHM of the diffraction maxima, and the square of the corresponding reciprocal

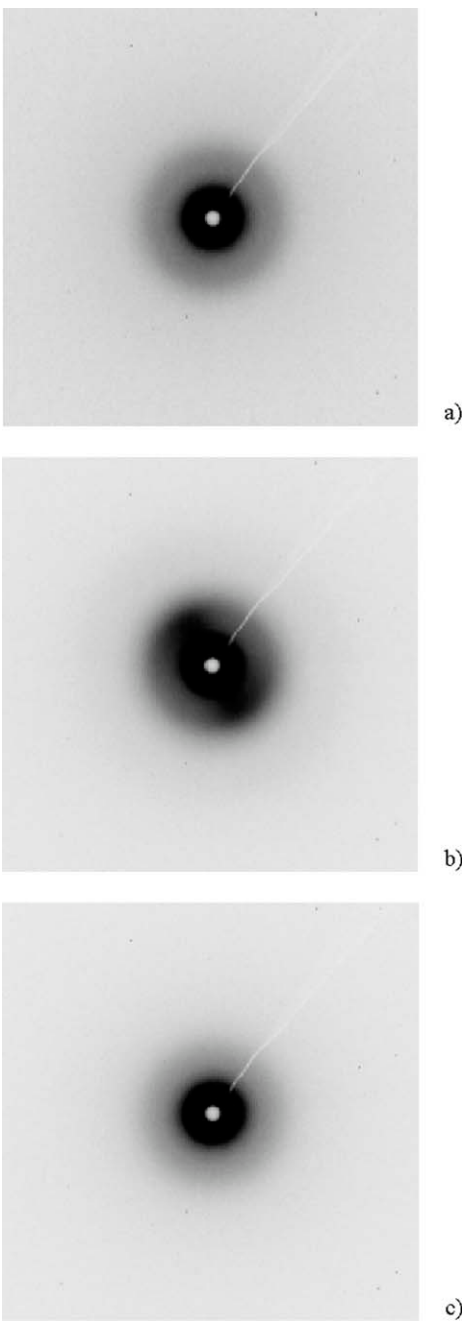

Figure 3 SAXS patterns of iPP: (a) originally untreated sample; (b) after crosslinking; (c) crosslinked + 2 wt % clay content.

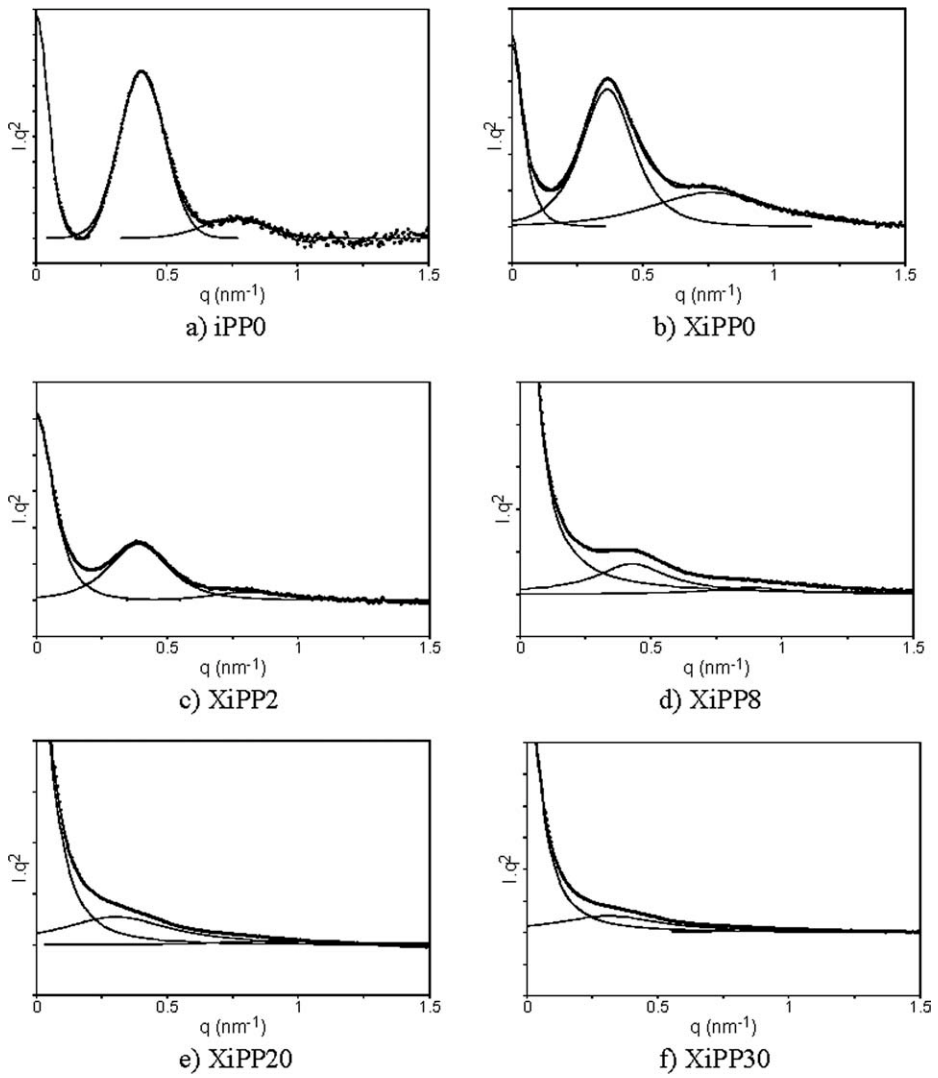

Figure 4 SAXS curves of iPP: (a) originally untreated sample; (b–f) crosslinked iPP with 0, 2, 8, 20, and 30 wt % of clay content.

vectors, b ($b = 2\ \sin\theta/\lambda = m/L$). This relationship is expressed by the equation[35]:

$$\delta\beta = 1/D_{\mathrm{SAXS}} + (\pi g m)^2/L \tag{2}$$

where m is the reflection order, and $g = \Delta L/L$ is the mean fluctuation of the long spacing. In addition, $\delta\beta$ is defined as:

$$\delta\beta = \lambda/cos\ \theta\ d\theta \tag{3}$$

where θ is the half of the diffraction angle, $d\theta$ is the FWHM of the diffraction maximum expressed in radians, and λ is the wavelength of the radiation. As mentioned above, the two maxima appearing in the SAXS patterns are not related to each other. Therefore, we have derived the D_{SAXS} values from the $\delta\beta$ value for the first reflection L_1. In cases where only one reflection is available, the formula for the calculation of D_{SAXS} taking into account the influence of paracrystalline distortions reduces to[34]:

$$D_{\mathrm{SAXS}} = (1/\pi^2\alpha^{*2})/\delta\beta \tag{4}$$

where the α^* value is given by:

$$\alpha^* = gN^{1/2} \tag{5}$$

which is the so-called α^*-law,[31] relating the number of N lattice planes of a paracrystal in a given direction with the relative mean fluctuation of the distance between these planes, g. In case of SAXS profiles, $N = D_{\mathrm{SAXS}}/L_1$ is the number of lamellae that contribute to the coherence length. Preceding studies indicate that the α^* value lies in the range between 0.1–0.2 for a variety of materials.[32,33] For the samples included in this study, we have taken $\alpha^* = 0.14$ as average value found for many polymers.[32,33]

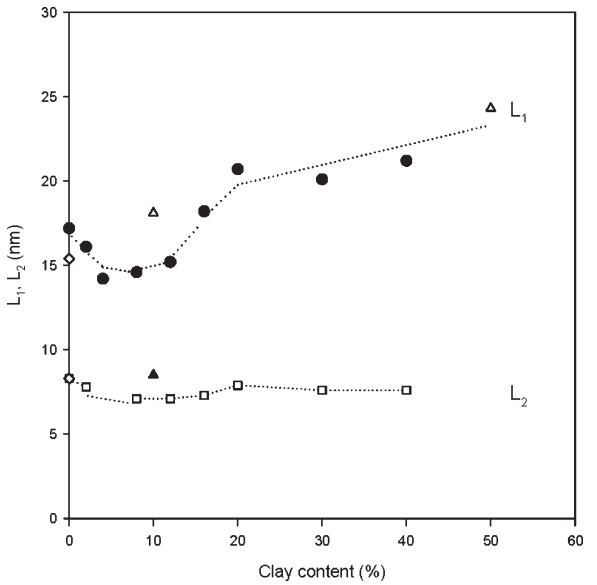

Figure 5 Clay content dependence of the long spacings: L_1 (●); L_2 (□); untreated sample (◇); samples prepared by *in situ* method: (▲, △).

From the SAXS profile analysis, we notice that the D_{SAXS} value derived from eq. (4) gradually decreases as the clay content increases; and for clay concentrations equal or larger than 16 wt %, D_{SAXS} is slightly higher than the value of the long spacing (Fig. 6).

DISCUSSION

The fact that the main (001) clay peak is shifted towards higher 2θ values for the composites suggests that the clay platelets are somehow collapsed within the iPP/clay composites, the *d*-spacing diminishing from 1.42 to 1.28 nm. This difference is higher than the experimental scattering of *d*-values. On the other hand, from the FWHM of this reflection, it is found that, whereas in the pure clay sample the average number of stacks in the perpendicular direction to this set of planes is 3–4, in the composites this number varies between 15 (sample with 2% of clay), and 9 (sample with 50% of clay). In most of composites the number of stacks is 12–13. As indicated in Figure 2 of our preceding study,[19] in samples with 30–50% clay content, the scattering intensity from the clay peak at 6.9° (2θ) increases with the clay concentration up to 10% of the total diffracted intensity. Thus, it seems that the blending process gives rise to an increase in the average number of clay platelets stacked together; however, only 10% of them (as a maximum) appear to be in a crystallographic register. Moreover, the sample with 4% of clay does not exhibit any clay peak in the WAXD diagram. This might be an indication of this sample showing complete exfoliation. In any case the intercalation of the material does not take place.

The β-form appearing in all samples can be related to the intense shearing originated in them as a consequence of the repeated extrusion cycles. In fact, several authors[36,37] indicate that when molten iPP is subjected to shear, the formation of the β-type crystals is favored. In addition, the β-form was thought to be responsible for the melting behavior shown by the samples with 16–30% of clay.[37] On the other hand, the appearance of the γ-form may be explained by the fact that, in the composites, the chain folding at the lamellae surface is made more difficult, first of all, by the crosslinking process itself, and secondly, by the presence of high amounts of clay.[30,38,39] Some authors have related the second maximum appearing in the SAXS patterns of iPP/clay composites with the presence in iPP of a certain amount of the γ-form.[38]

The intensity decrease of the main iPP peak in the WAXS diagrams with increasing clay content (Fig. 2) can be explained in terms of the decreasing amount of iPP that is gradually reduced down to 50%.

Concerning the SAXS results, one can think of the double orientation effect shown by the sample XiPP0 (crosslinked iPP with no clay) as originated by the crosslinking process. However, the presence of the clay has a disturbing effect, and does not allow this double orientation to take place (Fig. 4). In addition, the L_1 increase for clay contents higher than 16% (Fig. 5) could be related to the decrease of crystallinity observed in these compositions (Fig. 2 in Ref. 19). Both effects can be explained as due to the presence of increasing amounts of clay, which influences the crystallization ability of iPP, restricting somehow the

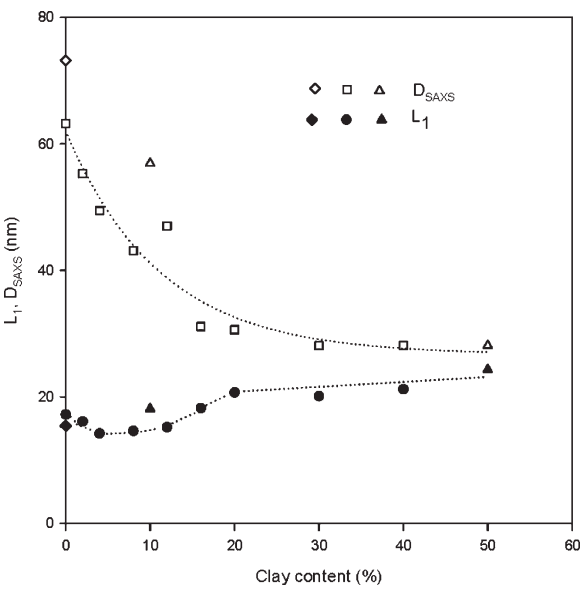

Figure 6 Comparison of the long spacing L_1 and the coherence length in lamellar stacks direction, D_{SAXS} as a function of clay content.

TABLE II
iPP/Clay Composites: Melting Points, T_c^{α} and T_c^{β} from DSC; Crystal Thickness Values l_C^{α} and l_C^{β} Derived from the Melting Points; Total Melting Enthalpy ΔHm and Crystallinity Values α_{DSC} and α_{WAXS}

Clay content	T_m^{α} (°C)	l_c^{α} (nm)	T_m^{β} (°C)	l_c^{β} (nm)	ΔH_m J/g	α_{DSC}	α_{WAXS}
Unmodified iPP	159.6	16.7	–	–	96.4	0.47	0.47
0	161.7	18.1	–	–	99.2	0.48	0.55
2	158.9	16.3	–	–	88.0	0.42	0.47
4	150.7	12.7	–	–	81.2	0.40	0.45
8	159.2	16.5	–	–	82.6	0.40	0.47
12	160.5	17.3	–	–	89.8	0.43	0.51
16	158.5	16.1	145.2	18.2	87.3	0.43	0.51
20	159.4	16.6	145.4	18.3	82.9	0.41	0.53
30	159.9	16.9	146.2	18.7	75.0	0.37	0.46
40	159.0	16.4	142.5	16.9	78.8	0.38	0.48
10	161.4	17.9	–	–	88.6	0.43	0.49
50	159.1	16.4	145.5	18.3	84.3	0.41	0.43

mobility of the iPP chains. However, the crystallinity variation is not enough as to explain the notable increase of the long spacing. On the other hand, the crystal thickness derived from the DSC study remains practically constant for all the studied samples[19] (Table II). Thus, it seems that, as the clay content rises, the amorphous region thickness increases as well. Taking into account that, as indicated in the experimental section, and as a consequence of the preparation method, the iPP chains become grafted onto the clay layers, therefore one could speculate that some of these clay layers are partially exfoliated and incorporated into the amorphous regions of iPP, thus giving rise to the observed L_1 increase. In addition, the coherence length D_{SAXS} decreases as the clay content increases, and, for clay contents equal or higher than 16% the values are not much higher than the long spacing (Fig. 6). From the ratio D_{SAXS}/L_1 the number N of lamellar stacks is obtained. Results show that N decreases from 5 for the non-crosslinked material with no clay down to approximately 1–2 for higher clay contents. This means that as the clay content increases, the iPP crystals become more and more isolated, surrounded by the iPP amorphous material which, in turn, is grafted onto the clay lamellae. It is noteworthy that the degree of distortion exhibited by the iPP lamellar stacks, measured through the g-variation, gradually increases with the clay content from $g = 0.06$ for the pristine iPP or $g = 0.07$ for the crosslinked iPP with no clay, up to $g = 0.12$ or 0.13 for the composites with clay contents of 40 and 50%. A more detailed explanation of this complex exfoliation mechanism, involving different types of reactions (redox reaction, grafting and crosslinking) is reported elsewhere.[20]

Additional results on the same composites obtained by FTIR and DMTA, not presented here, favor the above interpretation about the grafting of iPP chains onto the clay lamellae. Thus, in the FTIR study, two new sharp peaks appear at 923 and 769 cm^{-1}, that are associated to Si—O—C bonds created between the iPP chain and the tetrahedral structure of the inorganic Si—O—Si clay plane.[40] The obtained DMTA results show the appearance of two T_g values in the composite with 4% of clay, clearly demonstrating that the clay is completely exfoliated.[40] Similarly to the scheme represented in the article by D. Gournis and coworkers,[41] Figure 7 shows the morphology of the hybrid structure in case of total exfoliation. The FTIR and DMTA results will be the object of a coming paper.

CONCLUSIONS

1) The most relevant point is that the reported technique of crosslinking by reactive extrusion gives rise to a partial or total exfoliation (4 wt % clay) with absence of intercalated structure.
2) Most of the iPP/clay nanocomposites reported in this study show two SAXS maxima that are not related to each other. These SAXS maxima

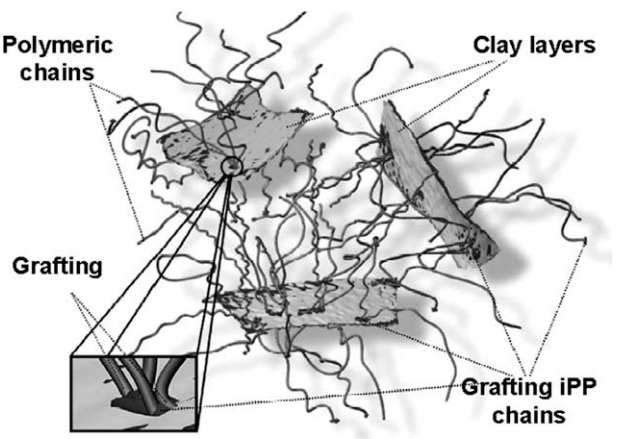

Figure 7 Illustration of the hybrid structure of totally exfoliated iPP/clay nanocomposite material.

have been associated to two polymorphic forms.

3) Analysis of the long spacing and the coherence length of the SAXS maxima of the composites reveals that the presence of increasing amounts of clay notably influences the lamellar stacking of the iPP lamellae, in such a way that the number of iPP crystals contributing to the lamellar stacks is reduced to about two units for the composites with the highest clay content.

References

1. Meyers, M. A.; Ritchie, R. O.; Sariyaka, M. Eds. Nano and Microstructural Design of Advanced Materials; Elsevier: Oxford, 2003.
2. Yuan, Q.; Awate, S.; Misra, R. D. K. Eur Polym J 2006, 42, 1994.
3. Chen, H.-S.; Chen, Ch.-M.; Chang, G.-Y.; Lee, S.-Y. Mater Chem Phys 2006, 96, 244.
4. Kiersnowski, A.; Chamczynska, J.; Trelinska-Wlazlak, M.; Lesniewicz, A.; Pigloswki, J. e-Polymers 2005, P_008, 1.
5. Kurian, M.; Galvin, M. E.; Trapa, P. E.; Sadoway, D. R.; Mayes, A. M. Electrochim Acta 2005, 50, 2125.
6. Vladimirov, V.; Betchev, C.; Vassiliou, A.; Papageorgiu, G.; Bikiaris, D. Comp Sci Technol 2006, 66, 2935.
7. Frounchi, M.; Dadbin, S.; Salehpour, Z.; Noferesti, M. J Membr Sci 2006, 282, 142.
8. Okada, A.; Usuki, A. Macromol Mat Eng 2006, 291, 1449.
9. Manias, E.; Touny, A.; Wu, L.; Strawhecker, K.; Lu, B.; Chung, T. C. Chem Mater 2001, 13, 3516.
10. Sinha Ray, S.; Okamoto, M. Prog Polym Sci 2003, 28, 1539.
11. Giannelis, E. P. Adv Mater 1996, 8, 29.
12. Reichert, P.; Nitz, H.; Klinke, S.; Brandtsch, R.; Thomann, R.; Mülhaupt, R. Macromol Mat Eng 2000, 275, 8.
13. Kawasumi, M.; Hasegawa, N.; Kato, M.; Usuki, A.; Okada, A. Macromolecules 1997, 30, 6333.
14. Rohlmann, C. O.; Failla, M. D.; Quinzani, L. M. Polymer 2006, 47, 7795.
15. Wong, S.-C.h; Lee, H.; Qu, S.; Mall, S.; Chen, L. Polymer 2006, 47, 7477.
16. Nowacki, R.; Monasse, B.; Piorkowska, E.; Galeski, A.; Haudin, J. M. Polymer 2004, 45, 4877.
17. Gelfer, M.; Burger, C.; Fadeev, A.; Sics, I.; Chu, B.; Hsiao, B. S.; Heintz, A.; Kojo, K.; Hsu, S.-L.; Si, M.; Rafailovich, M. Langmuir 2004, 20, 3746.
18. Shi, D.; Hu, G.-H.; Li, R. K. Y. J Chem Eng Sci 2006, 61, 3780.
19. Bouhelal, S.; Cagiao, M. E.; Khellaf, S.; Tabet, H.; Djellouli, B.; Benachour, D.; Baltá Calleja, F. J. J Appl Polym Sci 2010, 115, 2654.
20. Bouhelal, S.; Cagiao, M. E.; Bartolotta, A.; Di Marco, G.; Garrido, L.; Benachour, D.; Baltá Calleja, F. J. J Appl Polym Sci 2010, 116, 394.
21. Tanrattanakul, V.; Panwiriyarat, W. J Appl Polym Sci 2009, 114, 742.
22. Salavagione, H. J.; Cazorla-Amorós, D.; Tidjane, S.; Belbachir, M.; Benyoucef, M.; Morallón, E. Eur Polym J 2008, 44, 1275.
23. Bouhelal, S.; Cagiao, M. E.; Benachour, D.; Baltá Calleja, F. J. J Appl Polym Sci 2007, 103, 2968.
24. Bouhelal, S. U. S. Pat. 6,987,149 (2006).
25. Harpell, G. A.; Walrod, D. H. In Plastics Additives Handbook, 4th Ed.; Gatcher, R., Muller, H., Klemchuk, P. P., Eds.; Hanser: Munich, 1993; Chapter 17.
26. Karger-Kocsis, J., Ed. Polypropylene (Vol. 1: Structure, Blends and Composites), Chapman and Hall: London, 1995.
27. Meille, S. V.; Brückner, S. Nature 1989, 340, 455.
28. Meille, S. V.; Brückner, S.; Porzio, W. Macromolecules 1990, 23, 4114.
29. Turner Jones, A.; Aizlewood, J. M.; Becket, D. R. Makromol Chem 1964, 75, 134.
30. Nam, P. H.; Maiti, P.; Okamoto, M.; Kotaka, T.; Hasegawa, N.; Usuki, A. Polymer 2001, 42, 9633.
31. Olley, R. H.; Bassett, D. C. Polymer 1989, 30, 399.
32. Hosemann, R.; Hindeleh, A. M. J Macromol Sci Phys 1995, 34, 327.
33. Baltá Calleja, F. J.; Hosemann, R. J Appl Cryst 1980, 13, 521.
34. Santa Cruz, C. Superficies e interfases de materiales poliméricos. Estructura y microdureza, Ph. D. Thesis, Madrid, 1991.
35. Cabarcos, E. L.; Bermúdez, S. F.; Baltá Calleja, F. J. Colloid Polym Sci 1981, 259, 641.
36. Marigo, A.; Marega, C.; Causin, V.; Ferrari, P. J Appl Polym Sci 2004, 91, 1008.
37. Oitzi, J.; Skalicky, P. Polymer 1993, 34, 3168.
38. Causin, V.; Marega, C.; Marigo, A.; Ferrara, G.; Ferraro, A.; Selleri, R. J Nanosci Nanotechnol 2008, 8, 1823.
39. Maiti, P.; Nam, P. H.; Okamoto, M.; Kotaka, T.; Hasegawa, N.; Usuki, A. Polym Eng Sci 2002, 42, 1864.
40. Bouhelal, S.; Cagiao, M. E. Private communication. Unpublished results.
41. Gournis, D.; Karakassides, M. A.; Bakas, T.; Boukos, N.; Petridis, D. Carbon 2002, 40, 2641.